BIOCHEMISTRY
including biophysical chemistry & molecular biology

Article

pubs.acs.org/biochemistry

Modulation and Functional Role of the Orientations of the N- and P-Domains of Cu^+-Transporting ATPase along the Ion Transport Cycle

Dan Meng,[†] Lei Bruschweiler-Li,[†,§] Fengli Zhang,[‡] and Rafael Brüschweiler*[,†,§,‡]

[†]Department of Chemistry & Biochemistry, Florida State University, Tallahassee, Florida 32306, United States

[‡]National High Magnetic Field Laboratory, Tallahassee, Florida 32310, United States

[§]Department of Chemistry & Biochemistry, The Ohio State University, Columbus, Ohio 43210, United States

Supporting Information

ABSTRACT: Ion transport of different P-type ATPases is regulated similarly through the interplay of multiple protein domains. In the presence of ATP, binding of a cation to the ion binding site in the transmembrane helices leads to the phosphorylation of the P-domain, allowing ion transfer across the membrane. The details of the mechanism, however, are not clear. Here, we report the modulation of the orientation between the N- and P-domains of Cu^+-transporting ATPase along the ion transport cycle using high-resolution nuclear magnetic resonance spectroscopy in solution. On the basis of residual dipolar coupling measurements, it is found that the interdomain orientation (relative openness) of the N- and P-domains is distinctly modulated depending on the specific state of the N- and P-domains along the ion translocation cycle. The two domains' relative position in the apo state is semiopen, whereas it becomes closed upon binding of ATP to the N-domain. After phosphorylation of the P-domain and the release of ADP, the opening, however, becomes the widest among all the states. We reason such wide opening resulting from the departure of ADP prepares the N- and P-domains to accommodate the A-domain for interaction and, hence, promote ion transport and allow dephosphorylation of the P-domain. Such wide interdomain opening is abolished when an Asn to Asp mutation is introduced into the conserved DXXK motif located in the hinge region of the N- and P-domains of Cu^+-ATPase, suggesting the indispensible role of the N- and P-interdomain orientation during ion transportation. Our results shed new light on the structural and mechanistic details of P-type ATPase function at large.

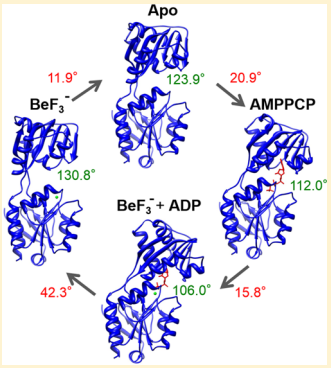

Copper is an essential cofactor for numerous enzymes with copper homeostasis being tightly controlled in all living cells. In human, the two Cu^+-transporting ATPases ATP7A and ATP7B are responsible for the regulation of the intracellular copper concentration. Their malfunction can result in Menkes disease[1] and Wilson disease,[2] respectively. Cu^+-transporting ATPases belong to the P_1B subfamily of P-type ATPases. Other prominent members of the P-type ATPase family include Na^+/K^+ ATPase and Ca^{2+} ATPase of skeletal muscle sarcoplasmic reticulum (SERCA), both of which belong to the P_2 subfamily.[3] During the ion transport cycle, P-type ATPases undergo a specific sequence of conformational transitions between the E1 and E2 states,[3−5] and the energy derived from ATP hydrolysis is utilized to achieve the active ion transport against a concentration gradient of the ion. A key invariant aspartate residue in the P-domain facing the ATP binding site in the N-domain is first autophosphorylated and later dephosphorylated during this cyclic process.

Crystal structures of SERCA have been reported for a number of different conformational states[6−11] as well as crystal structures of Cu^+-transporting ATPase and Na^+/K^+ ATPase.[12−19] The P-type ATPases share similar structures for the three cytoplasmic domains, including the nucleotide binding (N) domain, the phosphorylation (P) domain, and the actuator (A) domain. The current catalytic model of P-type ATPases relies largely on X-ray crystal structures and on mutagenesis of SERCA. The crystal structures capture snapshots of the different conformations of SERCA during the reaction cycle and help rationalize a number of important aspects of the mechanism of the active transport by SERCA. Basically, the catalytic cycle is composed of the following distinct steps: ATP binding, subsequent phosphorylation of the conserved Asp residue at the N-domain−P-domain interface, the release of ADP, the access of the A-domain for dephosphorylation, and the transport of the ion across the membrane. However, several key questions are left unanswered about the reaction cycle. One of them concerns the continuous communication along the different steps of the transport cycle.

In this work, we study the N- and P-domains of CopA from hyperthermophilic archaea *Archaeoglobus fulgidus* with high-resolution nuclear magnetic resonance (NMR) techniques to understand the functional interplay of these domains during the

Received: April 18, 2015
Revised: July 18, 2015
Published: July 21, 2015

DOI: 10.1021/acs.biochem.5b00420
Biochemistry 2015, 54, 5095−5102

translocation cycle of this ion transporter. The transmembrane helices, which provide cation binding sites, are represented in truncated form (Figure 1) in the absence of the A-domain.

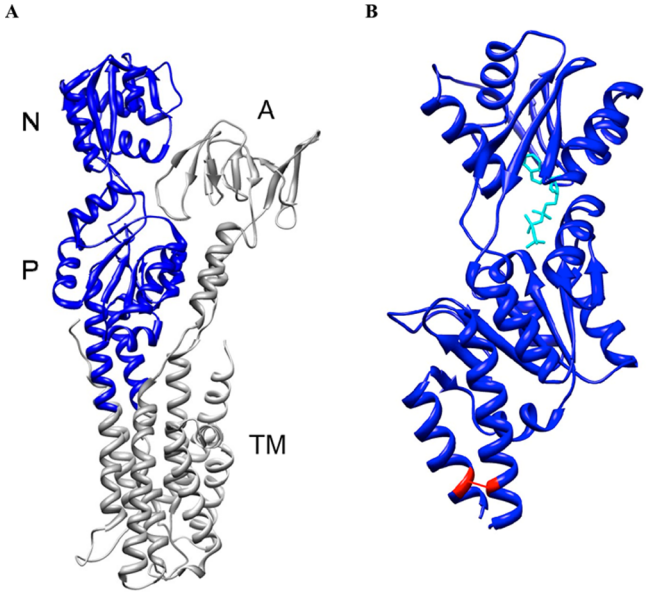

Figure 1. Overview of structures of CopA_NPwt and CopA_NPss. (A) Full length crystal structure of *Legionella pneumophila* CopA Cu-ATPase [Protein Data Bank (PDB) entry 3RFU]. The N- and P-domains of the CopA_NPwt construct are colored blue. The N-, P-, and A-domains and the transmembrane helices (TM) are labeled. (B) Structural model of CopA_NPss, with the N- and P-domains of *A. fulgidus* CopA (PDB entry 3A1C) and the extra N- and C-terminal helices (bottom) modeled using information from PDB entry 3RFU. The position of the double mutation, A391C and K671C, in CopA_NPss is colored red. AMPPCP is colored cyan.

Residual dipolar couplings (RDCs) were measured here to study the domain orientation for different states of the ion transportation cycle, based on structural information obtained by crystallography.[20−22] Previous NMR studies investigated the solution structure and dynamics of the N-domain and the N-terminal metal binding domain of human Cu ATPases.[23−31] The amino acid sequence arrangement of the N- and P-domains is P1 (amino acids A400−L429)−N (E435−S547)−P2 (S553−R666). The two segments of T430−P434 (between P1 and N) and D548−E552 (between N and P2) define the hinge region. RDC analysis of the D548N mutant in the conserved DXXK motif in the hinge region confirmed our notion that proper N- and P-interdomain orientation is critical for the function of P-type ATPase.

EXPERIMENTAL PROCEDURES

Cloning and Plasmid Constructions of CopA N- and P-Domains. The procedure for molecular cloning, protein expression, and purification was as previously reported.[32] The D548N mutant of CopA_NPss was generated using QuikChange Lightning Multi Site-Directed Mutagenesis Kit (Agilent) with the two primers of 5′-TTG AGG GGA TTA TAG CGG TTT CTA ACA CGC TCA AGG-3′ and 5′-CCT TGA GCG TGT TAG AAA CCG CTA TAA TCC CCT CAA-3′. The Qiagen kit was used for plasmid extraction, and the Eppendorf gel kit was used for gel extraction. The gene sequence of the coding region was verified by DNA sequencing (Applied Biosystems 3730 Genetic Analyzer).

Isothermal Titration Calorimetry (ITC). Titration experiments conducted via isothermal titration calorimetry (ITC) were performed at 25 °C using a VP-ITC microcalorimeter (MicroCal Inc., Northampton, MA). The calorimeter has a sample cell containing 1.45 mL of a protein solution and a matched thermal reference cell filled with water. Protein samples were buffer exchanged into 20 mM Hepes (pH 7.0), 100 mM NaCl, and 5 mM $MgCl_2$. The AMPPCP solution was also prepared in the same buffer at pH 7.0. Before each titration experiment, protein and AMPPCP solutions were filtered and degassed under vacuum for 10 min in a Thermo Vac system (MicroCal). Sixty 4 μL injections of the AMPPCP solution with at least 4 min intervals between injections were performed in protein. The syringe stirring speed was set to 310 rpm, and the reference power was 15 μcal/s. Baseline data were measured by titration of the AMPPCP solution into the buffer without protein and were subtracted from the experimental data. The protein concentration was determined by UV absorption using the theoretical extinction coefficient computed from the amino acid sequence. ITC data analysis was performed with Origin 7.0 provided by MicroCal.

Residual Dipolar Coupling (RDC) Experiments. Uniformly ^{15}N-labeled CopA_NPss samples in different states were used for RDC experiments. The apo sample was prepared with 1 mM CopA_NPss in 20 mM Hepes buffer (pH 7.0), 50 mM NaCl, and 10% D_2O. The AMPPCP-bound sample was prepared under the same condition and also included 10 mM AMPPCP and 5 mM $MgCl_2$. A phospho-aspartate mimic (BeF_3^--bound state) sample was prepared with 1 mM CopA_NPss in the buffer of 20 mM Hepes (pH 7.0), 100 mM NaF, 16 mM $BeCl_2$, 10 mM $MgCl_2$, and 10% D_2O.[33] The transition state sample (BeF_3^- and ADP-bound state) includes 1 mM CopA_NPss in the buffer of 20 mM Hepes (pH 7.0), 100 mM NaF, 16 mM $BeCl_2$, 10 mM $MgCl_2$, 50 mM ADP, and 10% D_2O. RDCs were determined from the analysis of ^{15}N HSQC and ^{15}N TROSY spectra[34] under the isotropic condition and aligned using 8 mg/mL Pf1 phage[35] (ASLA Biotech Ltd.) for the apo state, the AMPPCP-bound state, and the BeF_3^--bound state, and a 5.5% compressed polyacrylamide gel[36,37] (in house) for the BeF_3^- and ADP-bound state. Pf1 phage was heated at 50 °C for 5 min and cooled to room temperature before being gently mixed with CopA_NPss samples. Shigemi NMR tubes were used for the polyacrylamide gel samples. After the CopA_NPss had been mixed with the dried polyacrylamide gel, the tube was gently shaken until the gel was swollen. The tube was kept at room temperature for 2 days for the gel to swell homogeneously before NMR measurements were started.

The data were acquired at 313 K on a Bruker 800 MHz spectrometer equipped with a TCI cryoprobe. Data were processed using NMRpipe[38] and analyzed using Sparky.[39] Gaussian functions were used to fit the peaks in the ^{15}N HSQC and ^{15}N TROSY spectra to determine the peak positions. RDCs were fit to the apo and AMPPCP-bound CopA N- and P-domain crystal structures via singular-value decomposition (SVD)[40] using the MATLAB software. The calculation of the alignment tensor was performed for individual domains. The relative orientations of the N- and P-domains were determined as described previously.[41] Briefly, each domain was rotated separately, so that their coordinate reference frames coincided with the respective alignment tensor frames. After rotation, the P-domain was translated relative to the N-domain such that the Cα atom of the linker residue G432, which is close to the center of mass of the two linkers, coincided in both N- and P-

DOI: 10.1021/acs.biochem.5b00420
Biochemistry 2015, 54, 5095−5102

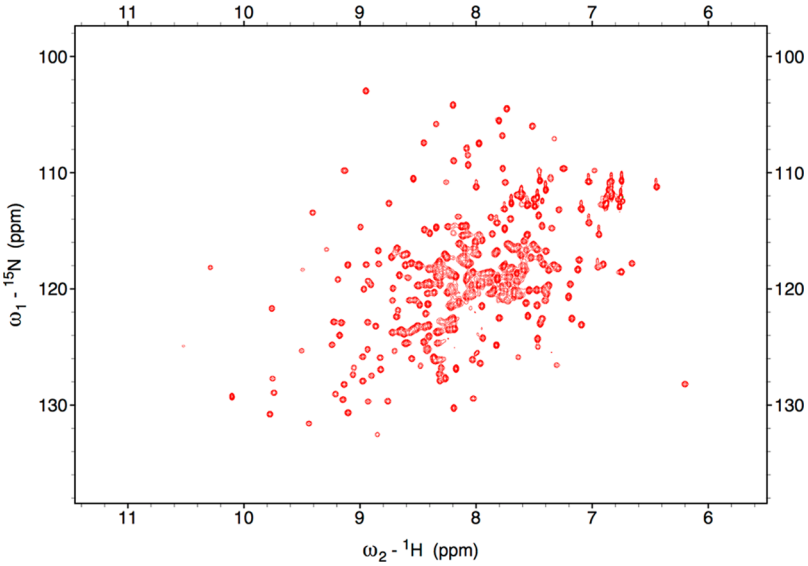

Figure 2. ^{1}H−^{15}N HSQC spectrum of uniformly ^{15}N-labeled CopA_NPss in the apo state. The spectrum was recorded at 800 MHz and 40 °C.

domains. Because of the invariance of dipolar couplings under inversion, the solution of the relative orientation is 4-fold degenerate, and hence, unrealistic solutions need to be identified and discarded on the basis of steric restrictions,[42,43] such as steric clashes between the domains.

Domain Opening Angle Computation. Three different metrics were used to evaluate the interdomain opening angle of CopA_NPss. In all analyses, the N-domain was defined as residues E435−S547. The linker region included residues T430−P434 and residues D548−E552. The P-domain includes residues A400−L429 and residues S553−R666. The interdomain opening angle is defined as the angle between two vectors, which are the vectors between the center of mass of all Cα atoms of the N-domain and the center of mass of all Cα atoms of the P-domain and the center of mass of the Cα atoms of the linker, respectively. The second metric calculates the average of the distance from each Cα atom of the N-domain to each Cα atom of the P-domain. In the third metric, the minimal distances from each Cα atom of the N-domain to each Cα atom of the P-domain were calculated. The median of the minimal distances was subsequently determined. MATLAB software was used for all these calculations. Monte Carlo error analysis was performed by adding Gaussian noise with a standard deviation of 1.0 Hz to the experimental RDCs, which was repeated 300 times. The resulting 300 RDC sets were then used for the computation of the interdomain opening angle and its standard deviation. The rotation angle of the N-domain relative to the P-domain from one state to another was determined in Chimera (Chimera UCSF).

RESULTS

CopA_NPss as a Model System for N- and P-Domains. The Cu^{+}-ATPase construct used in this work consists of the N- and P-domains comprising the contiguous amino acid sequence A387−N675 of CopA from hyperthermophilic archaea *A. fulgidus* (CopA_NPwt), which amounts to a molecular weight of 31 kDa (Figure 1A). The crystal structure of a similar construct consisting of residues K398−K673 has been reported previously.[22] We recorded ^{1}H−^{15}N HSQC NMR spectra of uniformly ^{15}N-labeled CopA_NPwt in solution to assess the structure and dynamics of the protein. Even at 40 °C, the spectra displayed considerable peak broadening leading to substantial cross-peak overlap. This broadening behavior could be considerably reduced by the introduction of a double mutant of CopA_NPwt with A391C and K671C mutations located in the N- and C-terminal helices of the P-domain, which is termed CopA_NPss. The introduction of these two cysteine residues at these locations was inspired by the crystal structure of the intact molecule in which these two residues are very close in space. With the addition of this disulfide bond (Figure 1B), this truncated version of the protein is expected to assume a structure that resembles its counterpart in intact CopA. The presence of the disulfide bond was unambiguously confirmed by sodium dodecyl sulfate−polyacrylamide gel electrophoresis (Figure S1). CopA_NPss displayed very well resolved cross-peaks in the ^{1}H−^{15}N HSQC spectrum at 40 °C (Figure 2). Therefore, a disulfide linkage of the N- and C-terminal helices stabilizes a state of the N- and P-domains that is better organized on the NMR chemical shift time scale (i.e., the millisecond time scale).

Backbone resonance assignments of CopA_NPss in the apo and ATP analogue AMPPCP-bound states were obtained using standard three-dimensional triple-resonance NMR experiments.[32] The secondary structures of CopA_NPss in solution in both AMPPCP free and bound states were identified using TALOS-N[44] (Figure 3). Overall, the secondary structures matched those of the crystal structures. Some differences between the secondary structures in the crystal and in solution are observed, which are likely due to the fraying effects, presumably reflecting the large temperature difference between solution NMR (313 K) and X-ray crystallography (100 K). On the basis of two-dimensional HSQC spectra, the chemical shift perturbation observed indicates that CopA_NPss is able to bind AMPPCP (Figure S2). Furthermore, the chemical shift differences of CopA_NPss between nucleotide free and bound states suggest that AMPPCP binding perturbs the nucleotide binding site and the N- and C-terminal linkers. The apparent dissociation constant measured by isothermal titration calorimetry was 0.26 mM (Figure S3), which is similar to that reported for the N- and P-domains of CopA (K_d ∼ 0.1 mM).[22] This further confirmed that CopA_NPss is as active as CopA_NPwt.

DOI: 10.1021/acs.biochem.5b00420
Biochemistry 2015, 54, 5095−5102

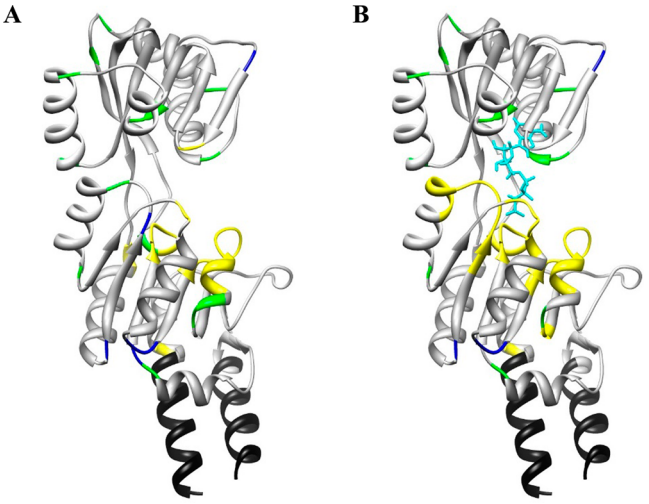

Figure 3. Secondary structure differences between the X-ray crystal structure and NMR solution structure of CopA_NPss in (A) the apo state and (B) the AMPPCP-bound state mapped onto crystal structure of Protein Data Bank entry 3A1C. Identical secondary structures determined by both methods are colored gray; β-strands by NMR, but not X-ray, blue; loops by NMR, but not X-ray, green; residues not assigned yellow; and residues not used for comparison black. AMPPCP is colored cyan.

Domain Orientation of CopA_NPss. The interdomain orientations of CopA_NPss in solution were derived from experimental backbone $^{1}H-^{15}N$ residual dipolar couplings (RDCs). RDCs reflect the average orientation of $^{1}H-^{15}N$ bonds with respect to the external magnetic field, and they are exquisitely sensitive to the relative average orientation of protein domains. This information can be used to characterize the orientations of individual domains of a multidomain protein relative to a common alignment tensor[45−50] by singular-value decomposition (SVD).[40] Around 80 dipolar couplings for the N-domain and around 60 dipolar couplings for the P-domain were measured after the protein was weakly aligned in 8 mg/mL Pf1 phage in the apo state, the AMPPCP-bound state, and the BeF_3^--bound state (mimicking the phosphorylated state after ADP has been released). Around 60 dipolar couplings could be measured for the N- and P-domains when using a 5.5% compressed polyacrylamide gel for the BeF_3^- and ADP-bound transition state analogue (mimicking the phosphorylated state in the presence of ADP). Both the apo and AMPPCP-bound crystal structures [Protein Data Bank (PDB) entries 2B8E, 2.3 Å, and 3A1C, 1.8 Å] were used to fit the RDCs. The level of agreement between experimental RDCs and calculated RDCs based on the crystal structures was evaluated in terms of a Q value.[51] Crystal structure 3A1C was used for the determination of domain orientations because it has better resolution and the derived Q values are smaller (i.e., better) (Table S1 and Figure S4), indicative of good agreement between the structures of the individual domains in the crystal and in solution. The N- and P-domain Q values remain essentially the same regardless of whether the linker residues between the two domains were included in or excluded from the calculation (Table S2). This indicates that the linker structure of crystal structure 3A1C is representative for both the apo and AMPPCP-bound states. The calculated alignment tensor magnitudes and rhombicities of CopA_NPss in different states are shown in Table S3, and the experimental RDCs are included in Table S4. CopA_NPss is very rigid even in the apo state as suggested by the relaxation data (Figure S5), thus allowing the RDC-based characterization of the interdomain orientation of a multidomain protein. The domain orientations in solution in the apo and AMPPCP-bound states were quite similar to the crystal structures reported (Figure S6). The Cα root-mean-square deviations (rmsd) between the solution and the crystal structure in the apo and AMPPCP-bound states are 2.01 and 0.43 Å, respectively.

In solution, the apo state populates on average a state more open than the one displayed by the crystal structure, with an interdomain opening angle of 123.9°. As shown in Figure 4,

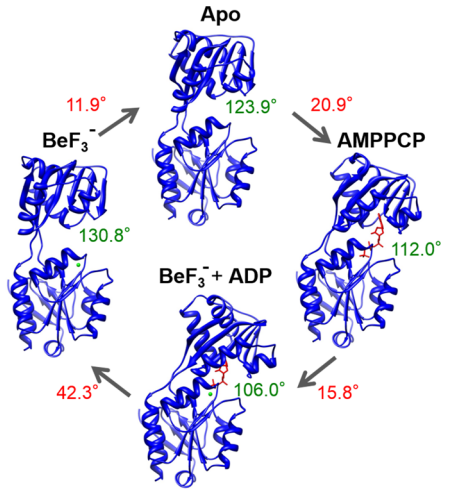

Figure 4. Interdomain orientations of CopA_NPss in the catalytic reaction cycle determined by NMR RDCs. The interdomain opening angles are indicated in green. The rotation angles of the N-domain relative to the P-domain between states are indicated in red. AMPPCP and ADP molecules are colored red. BeF_3^- is indicated as a small green sphere. Because the rotation axes change between pairs of structures, the rotation angles are given as positive numbers only.

AMPPCP binding closes CopA_NPss by rotating the N-domain by 20.9°, resulting in an interdomain opening angle of only 112.0°. BeF_3^- and ADP binding in the catalytic site, which represents a mimetic of the transition state, further closes CopA_NPss by rotating the N-domain by 15.8°, leading to an opening angle of 106.0°. As ADP is being released from the binding pocket, the N-domain opens by a 42.3° rotation, resulting in an interdomain opening angle of 130.8° of the phosphorylated state of CopA_NPss as mimicked by BeF_3^- binding. This dramatic opening of CopA_NPss after the release of ADP indicates that phosphorylation of the P-domain promotes the opening of the N- and P-domains. This is functionally highly relevant as it gives the A-domain better access to the phosphorylation site of the P-domain (vide infra). After the P-domain has been dephosphorylated, CopA_NPss relaxes back to the apo state by rotation of the N-domain by 11.9°. In addition to the domain opening angle determination, the overall compactness of CopA_NPss was also characterized by calculating the average distance of each Cα atom of the N-domain to each Cα atom of the P-domain (Table 1). Moreover, the median minimal distance was determined as the median of the minimal distance of each Cα atom of the N-domain to each Cα atom of the P-domain. The three metrics are complementary to each other and should not be directly compared. Rather, each metric can be used to monitor the changes for different protein states. The three different methods used to

DOI: 10.1021/acs.biochem.5b00420
Biochemistry 2015, 54, 5095−5102

Table 1. Interdomain Opening of CopA_NPss in Different States Using Different Metrics[a]

	opening angle (deg)[b]	distance (Å)[c]	median minimal distance (Å)[d]
apo	123.9 ± 0.5	35.0 ± 0.1	18.1 ± 0.1
AMPPCP	112.0 ± 0.7	34.1 ± 0.2	17.4 ± 0.3
BeF_3^- and ADP	106.0 ± 1.0	33.2 ± 0.2	16.4 ± 0.3
BeF_3^-	130.8 ± 0.6	36.2 ± 0.1	20.0 ± 0.2

[a]The errors were calculated using Monte Carlo error analysis with a standard deviation of the RDCs of 1 Hz. [b]The opening angle is the angle between two vectors. One vector points from the center of mass of the Cα atoms of the linker to the center of mass of all Cα atoms of the N-domain. The other vector points from the center of mass of the Cα atoms of the linker to the center of mass of all Cα atoms of the P-domain. [c]Distance calculated as the average distance from each Cα atom of the N-domain to each Cα atom of the P-domain. [d]The median minimal distance is the median of the minimal distance of each Cα atom of the N-domain to each Cα atom of the P-domain.

evaluate the changes of the interdomain opening of CopA_NPss during the translocation cycle all show that the N- and P-domains gradually close when cycling from the apo state to the AMPPCP-bound state and to the transition state and then substantially open in the phosphorylated state in the absence of ADP.

Critical Point Mutation Highlights the Importance of NP Domain Orientation for Function. Because the N-domain is an insertion between two fragments of the P-domain, there are two hinge regions connecting the N- and P-domains. The C-terminal hinge region contains a conserved DXXK motif (amino acids D1230−K1233 for human ATP7A and amino acids D548−K551 for *A. fulgidus* CopA) in the Cu-ATPase (Figure S7), and the equivalent motif in SERCA is ^{601}DPPR (amino acids D601−R604). It has been proposed that the ^{601}DPPR motif in SERCA, which is part of the conserved segment of residues 601−624 that comprises the C-terminal hinge region and part of the P-domain, might be important for the proper coordination of the events in the N- and P-domains during the phosphorylation process.[11] Mutation studies of the conserved D601 residue in the hinge of SERCA showed that D601A and D601N mutations abolished Ca^{2+} translocation by disturbing the E1P to E2P conformational transition (where E1P and E2P denote the phosphorylated forms of states E1 and E2, respectively).[52] Interestingly, for the equivalent D1230A mutant in the human Cu-ATPase, ATP7A, Cu^+ transport activity was dramatically decreased, although the catalytic turnover of ATP was unaffected.[53] This suggests that the D1230A mutation somehow decouples the conformational changes during the catalytic cycle that link ATP hydrolysis and ion translocation in P-type ATPases. However, how the DPPR/DXXK motif coordinates the conformational transitions in the catalytic cycle remains unanswered.

We produced a D548N mutant based on CopA_NPss by site-directed mutagenesis. The binding affinity of AMPPCP in the presence of Mg^{2+} was obtained by isothermal titration calorimetry (ITC) for the D548N mutant (Figure S8). Not surprisingly, the D548N mutation resulted in a nearly 5-fold increase of the binding affinity for AMPPCP compared with that of CopA_NPss: the dissociation constant is 58 μM for the D548N mutant and 261 μM for CopA_NPss, a phenomenon observed in other P-type ATPase members when the Asp to Asn substitution was introduced into the conserved motif. For example, in SERCA, the D601N mutation in the DPPR motif showed enhanced ATP binding affinity,[52] and in the D1230A mutation in the DXXK motif of ATP7A, the ATP binding affinity increased by ∼20-fold.[53]

We then investigated the changes in interdomain orientation induced by the D548N mutation based on backbone ^{1}H−^{15}N residual dipolar coupling (RDC) experiments of CopA_NPss aligned in 8 mg/mL Pf1 phage. In the D548N mutant, more than 40 RDCs were obtained for each of the N- and P-domains in both AMPPCP free and AMPPCP-bound states. These dipolar couplings were fitted to both the reported apo and AMPPCP-bound crystal structures (PDB entries 2B8E, 2.3 Å, and 3A1C, 1.8 Å), and a Q value was calculated to evaluate the agreement between the experimental RDCs and the crystal structure (Tables S5 and S6 and Figure S9). Again, crystal structure 3A1C was used for the determination of the relative domain orientations. The low Q values for the individual domains (in the apo state, $Q = 0.32$ for the N-domain and $Q = 0.34$ for the P-domain; in the AMPCP-bound state, $Q = 0.41$ for the N-domain and $Q = 0.28$ for the P-domain) and the small chemical shift perturbations indicate that the D548N mutation causes little structural perturbation in the two domains. The interdomain orientations of the D548N mutant in both apo and AMPPCP-bound states behave much like that of CopA_NPss with backbone Cα rmsds of 0.25 and 0.26 Å in the apo and ligand-bound states (Figure S10), respectively. Therefore, the D548N mutation does not significantly alter the relative interdomain orientation in the apo and AMPPCP-bound states.

In the BeF_3^--bound state, the D548N mutant is more closed than wild-type CopA_NPss with a backbone Cα rmsd of 1.23 Å (Figure S10). The D548N mutant has an interdomain opening angle of 125.6° (Table 2), whereas the CopA_NPss counterpart has an interdomain angle of 130.8° (Table 1). This means that when the P-domains of these two systems are superimposed, the N-domains are rotated relative to each other by 11.6°. Importantly, the interdomain orientation of the D548N mutant in the BeF_3^--bound state is identical to that of this mutant in its apo state, which is also very similar to the wild-type apo form. Therefore, the wide opening of the N- and P-domain interface as a result of phosphorylation, as seen in CopA_NPss, is lost in the D548N mutant.

Table 2. Interdomain Opening of the D548N Mutant in Different States Using the Same Metrics That Are Used for CopA_NPss (Table 1)[a]

	opening angle (deg)	distance (Å)	median minimal distance (Å)
apo	125.3 ± 0.8	35.2 ± 0.2	18.7 ± 0.3
AMPPCP	112.1 ± 1.1	34.0 ± 0.2	17.0 ± 0.5
BeF_3^-	125.6 ± 0.9	35.4 ± 0.1	19.0 ± 0.3

[a]The error is calculated using Monte Carlo error analysis assuming a standard deviation of the RDCs of 1 Hz.

DISCUSSION

Domain Orientations in the Catalytic Cycle. The N- and P-domains of Cu-ATPase have been studied here using NMR to understand their structural properties in solution in relationship to their function. The overall structure of CopA_NPss in solution closely matches the crystal structures. The interdomain orientation of CopA_NPss was determined

DOI: 10.1021/acs.biochem.5b00420
Biochemistry 2015, 54, 5095−5102

from RDCs, which precisely report the average orientation in solution. Although there are many substates of CopA ATPase in the catalytic cycle, the relative orientation of the N- and P-domains can be described with four principal structures as shown in Figure 4. Comparing our RDC-derived structures with existing crystal structures indicates that the overall agreement is good, suggesting our system and method could faithfully represent general structure consensus. A detailed analysis, however, provided valuable new information about the underlying mechanism of P-type ATPase. Our RDC-derived AMPPCP and BeF_3^- plus ADP-bound states are very similar to the crystal structures (PDB entries 1T5S, 1VFP, 1T5T, and 2ZBD). Our apo state structure is close to the apo crystal structure of CopA (PDB entry 2B8E). Although it is more compact than the corresponding structure of SERCA (PDB entry 1SU4) in the Ca_2E1 open conformation with no ATP bound, as noted by Toyoshima this SERCA structure, however, is unlikely to represent the dominant state in solution, because an electron microscopy investigation of crystals generated under milder conditions showed the N- and P-domains to be more compact.[54] Further comparison indicates in the BeF_3^--bound state, the relative openness between the N- and P-domains in solution is not as wide as that in the crystal structure of CopA in the AlF_4^--bound state (PDB entry 3RFU), where the A-domain inserts deeply into the cleft between the N- and P-domains by rotating with respect to its apo state, which results in a conformational change in the transmembrane part allowing for ion translocation. This suggests that our RDC structure of the BeF_3^--bound state captured the moment when the N- and P-domains open after phosphorylation as well as ADP departure and are poised to interact with the A-domain, indicating initial N- and P-domain opening does not require the A-domain. Rather, it is the phosphorylation that triggered the N- and P-domain conformational change to ensure subsequent A-domain rotation and ion transport. Any disruption of the N- and P-domain opening process would significantly impair the function of the protein. When the A-domain is present at the N- and P-domain interface, the latter two domains can further open until the functionally important TGES loop of the A-domain is in the required position for dephosphorylation.

Role of the Conserved DXXK Motif. The DXXK motif in the hinge of the N- and P-domains allosterically regulates the ion translocation of the ATPase. In the human Cu-ATPase, ATP7A, the D1230A mutation in the DXXK motif causes a significant reduction in the level of copper translocation.[53] A similar allosteric role of the equivalent DPPR motif was observed in SERCA. Both D601N and D601E mutations in SERCA cause a reduction in the rate of phosphorylation by ATP, and Ca^{2+} translocation was disturbed as the rate of the conformational transition from the E1P state to the E2P state was reduced.[52] How such a single mutation resulted in the impairment of ion translocation remains an open question. Our results on the N- and P-domain orientation prompted us to look for an answer along this direction. We set out to make a mutation of D548N in the DXXK motif and measured RDCs of its apo state, AMPPCP-bound state, and BeF_3^--bound state. While the opening angle remains almost unchanged in the first two states, the opening angle in the BeF_3^--bound state is indeed smaller than that of the wild type, supporting the idea that the Asp to Asn substitution hinders the opening of the N- and P-domains after the phosphorylation event. Moreover, because the binding affinity of ATP analogues in the mutant is much higher than in wild-type (WT) CopA, strong binding affinity is expected for ADP, as well. After phosphorylation, it is therefore likely that in the mutant, but not the WT, ADP becomes sterically stuck in the nucleotide binding pocket, thereby reducing the openness between the N- and P-domains. Mutation analysis further confirmed our hypothesis that the N- and P-domain orientation is critical for the proper function of the P-type ATPase.

■ ASSOCIATED CONTENT

Supporting Information

The Supporting Information is available free of charge on the ACS Publications website at DOI: 10.1021/acs.biochem.5b00420.

Tables with RDCs and analysis results and figures with experimental results, CopA structures, and interdomain orientations (PDF)

■ AUTHOR INFORMATION

Corresponding Author

*E-mail: bruschweiler.1@osu.edu. Telephone: +1 (614) 688-2083.

Funding

This work was supported by the National Science Foundation (Grant MCB 1360966).

Notes

The authors declare no competing financial interest.

■ ACKNOWLEDGMENTS

We are thankful for the technical support and discussion by Drs. Xiaogang Niu and Dawei Li.

■ REFERENCES

(1) Vulpe, C., Levinson, B., Whitney, S., Packman, S., and Gitschier, J. (1993) Isolation of a candidate gene for Menkes disease and evidence that it encodes a copper-transporting ATPase. *Nat. Genet. 3*, 7−13.

(2) Bull, P. C., Thomas, G. R., Rommens, J. M., Forbes, J. R., and Cox, D. W. (1993) The Wilson disease gene is a putative copper transporting P-type ATPase similar to the Menkes gene. *Nat. Genet. 5*, 327−337.

(3) Kühlbrandt, W. (2004) Biology, structure and mechanism of P-type ATPases. *Nat. Rev. Mol. Cell Biol. 5*, 282−295.

(4) Albers, R. W., Fahn, S., and Koval, G. J. (1963) The Role of Sodium Ions in the Activation of Electrophorus Electric Organ Adenosine Triphosphatase. *Proc. Natl. Acad. Sci. U. S. A. 50*, 474−481.

(5) Post, R. L., and Sen, A. K. (1965) An Enzymatic Mechanism of Active Sodium and Potassium Transport. *J. Histochem. Cytochem. 13*, 105−112.

(6) Olesen, C., Picard, M., Winther, A. M., Gyrup, C., Morth, J. P., Oxvig, C., Møller, J. V., and Nissen, P. (2007) The structural basis of calcium transport by the calcium pump. *Nature 450*, 1036−1042.

(7) Sørensen, T. L., Møller, J. V., and Nissen, P. (2004) Phosphoryl transfer and calcium ion occlusion in the calcium pump. *Science 304*, 1672−1675.

(8) Toyoshima, C., Nakasako, M., Nomura, H., and Ogawa, H. (2000) Crystal structure of the calcium pump of sarcoplasmic reticulum at 2.6 angstrom resolution. *Nature 405*, 647−655.

(9) Toyoshima, C., and Nomura, H. (2002) Structural changes in the calcium pump accompanying the dissociation of calcium. *Nature 418*, 605−611.

(10) Toyoshima, C., Nomura, H., and Tsuda, T. (2004) Lumenal gating mechanism revealed in calcium pump crystal structures with phosphate analogues. *Nature 432*, 361−368.

DOI: 10.1021/acs.biochem.5b00420
Biochemistry 2015, 54, 5095−5102

(11) Møller, J. V., Olesen, C., Winther, A. M., and Nissen, P. (2010) The sarcoplasmic Ca2+-ATPase: design of a perfect chemi-osmotic pump. *Q. Rev. Biophys. 43*, 501−566.
(12) Andersson, M., Mattle, D., Sitsel, O., Klymchuk, T., Nielsen, A. M., Møller, L. B., White, S. H., Nissen, P., and Gourdon, P. (2013) Copper-transporting P-type ATPases use a unique ion-release pathway. *Nat. Struct. Mol. Biol. 21*, 43−48.
(13) Gourdon, P., Liu, X. Y., Skjørringe, T., Morth, J. P., Møller, L. B., Pedersen, B. P., and Nissen, P. (2011) Crystal structure of a copper-transporting PIB-type ATPase. *Nature 475*, 59−64.
(14) Kanai, R., Ogawa, H., Vilsen, B., Cornelius, F., and Toyoshima, C. (2013) Crystal structure of a Na+-bound Na+,K+-ATPase preceding the E1P state. *Nature 502*, 201−206.
(15) Laursen, M., Yatime, L., Nissen, P., and Fedosova, N. U. (2013) Crystal structure of the high-affinity Na+K+-ATPase-ouabain complex with Mg2+ bound in the cation binding site. *Proc. Natl. Acad. Sci. U. S. A. 110*, 10958−10963.
(16) Morth, J. P., Pedersen, B. P., Toustrup-Jensen, M. S., Sørensen, T. L., Petersen, J., Andersen, J. P., Vilsen, B., and Nissen, P. (2007) Crystal structure of the sodium-potassium pump. *Nature 450*, 1043−1049.
(17) Nyblom, M., Poulsen, H., Gourdon, P., Reinhard, L., Andersson, M., Lindahl, E., Fedosova, N., and Nissen, P. (2013) Crystal structure of Na+, K(+)-ATPase in the Na(+)-bound state. *Science 342*, 123−127.
(18) Ogawa, H., Shinoda, T., Cornelius, F., and Toyoshima, C. (2009) Crystal structure of the sodium-potassium pump (Na+,K+-ATPase) with bound potassium and ouabain. *Proc. Natl. Acad. Sci. U. S. A. 106*, 13742−13747.
(19) Shinoda, T., Ogawa, H., Cornelius, F., and Toyoshima, C. (2009) Crystal structure of the sodium-potassium pump at 2.4 A resolution. *Nature 459*, 446−450.
(20) Sazinsky, M. H., Mandal, A. K., Argüello, J. M., and Rosenzweig, A. C. (2006) Structure of the ATP binding domain from the Archaeoglobus fulgidus Cu+-ATPase. *J. Biol. Chem. 281*, 11161−11166.
(21) Sazinsky, M. H., Agarwal, S., Argüello, J. M., and Rosenzweig, A. C. (2006) Structure of the actuator domain from the Archaeoglobus fulgidus Cu(+)-ATPase. *Biochemistry 45*, 9949−9955.
(22) Tsuda, T., and Toyoshima, C. (2009) Nucleotide recognition by CopA, a Cu+-transporting P-type ATPase. *EMBO J. 28*, 1782−1791.
(23) Banci, L., Bertini, I., Cantini, F., Inagaki, S., Migliardi, M., and Rosato, A. (2010) The binding mode of ATP revealed by the solution structure of the N-domain of human ATP7A. *J. Biol. Chem. 285*, 2537−2544.
(24) Dmitriev, O., Tsivkovskii, R., Abildgaard, F., Morgan, C. T., Markley, J. L., and Lutsenko, S. (2006) Solution structure of the N-domain of Wilson disease protein: distinct nucleotide-binding environment and effects of disease mutations. *Proc. Natl. Acad. Sci. U. S. A. 103*, 5302−5307.
(25) Gitschier, J., Moffat, B., Reilly, D., Wood, W. I., and Fairbrother, W. J. (1998) Solution structure of the fourth metal-binding domain from the Menkes copper-transporting ATPase. *Nat. Struct. Biol. 5*, 47−54.
(26) Banci, L., Bertini, I., Del Conte, R., D'Onofrio, M., and Rosato, A. (2004) Solution structure and backbone dynamics of the Cu(I) and apo forms of the second metal-binding domain of the Menkes protein ATP7A. *Biochemistry 43*, 3396−3403.
(27) Banci, L., Bertini, I., Cantini, F., Chasapis, C. T., Hadjiliadis, N., and Rosato, A. (2005) A NMR study of the interaction of a three-domain construct of ATP7A with copper(I) and copper(I)-HAH1: the interplay of domains. *J. Biol. Chem. 280*, 38259−38263.
(28) Banci, L., Bertini, I., Cantini, F., Della-Malva, N., Migliardi, M., and Rosato, A. (2007) The different intermolecular interactions of the soluble copper-binding domains of the menkes protein, ATP7A. *J. Biol. Chem. 282*, 23140−23146.
(29) Banci, L., Bertini, I., Cantini, F., Rosenzweig, A. C., and Yatsunyk, L. A. (2008) Metal binding domains 3 and 4 of the Wilson disease protein: solution structure and interaction with the copper(I) chaperone HAH1. *Biochemistry 47*, 7423−7429.
(30) Achila, D., Banci, L., Bertini, I., Bunce, J., Ciofi-Baffoni, S., and Huffman, D. L. (2006) Structure of human Wilson protein domains 5 and 6 and their interplay with domain 4 and the copper chaperone HAH1 in copper uptake. *Proc. Natl. Acad. Sci. U. S. A. 103*, 5729−5734.
(31) Fatemi, N., Korzhnev, D. M., Velyvis, A., Sarkar, B., and Forman-Kay, J. D. (2010) NMR characterization of copper-binding domains 4−6 of ATP7B. *Biochemistry 49*, 8468−8477.
(32) Meng, D., Bruschweiler-Li, L., Zhang, F., and Brüschweiler, R. (2015) NMR backbone resonance assignments of the N, P domains of CopA, a copper-transporting ATPase, in the apo and ligand bound states. *Biomol. NMR Assignments 9*, 129−133.
(33) Cho, H. S., Lee, S. Y., Yan, D., Pan, X., Parkinson, J. S., Kustu, S., Wemmer, D. E., and Pelton, J. G. (2000) NMR structure of activated CheY. *J. Mol. Biol. 297*, 543−551.
(34) Kontaxis, G., Clore, G. M., and Bax, A. (2000) Evaluation of cross-correlation effects and measurement of one-bond couplings in proteins with short transverse relaxation times. *J. Magn. Reson. 143*, 184−196.
(35) Hansen, M. R., Mueller, L., and Pardi, A. (1998) Tunable alignment of macromolecules by filamentous phage yields dipolar coupling interactions. *Nat. Struct. Biol. 5*, 1065−1074.
(36) Tycko, R., Blanco, F. J., and Ishii, Y. (2000) Alignment of biopolymers in strained gels: A new way to create detectable dipole-dipole couplings in high-resolution biomolecular NMR. *J. Am. Chem. Soc. 122*, 9340−9341.
(37) Sass, H. J., Musco, G., Stahl, S. J., Wingfield, P. T., and Grzesiek, S. (2000) Solution NMR of proteins within polyacrylamide gels: Diffusional properties and residual alignment by mechanical stress or embedding of oriented purple membranes. *J. Biomol. NMR 18*, 303−309.
(38) Delaglio, F., Grzesiek, S., Vuister, G. W., Zhu, G., Pfeifer, J., and Bax, A. (1995) NMRPipe: a multidimensional spectral processing system based on UNIX pipes. *J. Biomol. NMR 6*, 277−293.
(39) Goddard, T. D., and Kneller, D. G. (2004) *SPARKY 3*, University of California, San Francisco.
(40) Losonczi, J. A., Andrec, M., Fischer, M. W., and Prestegard, J. H. (1999) Order matrix analysis of residual dipolar couplings using singular value decomposition. *J. Magn. Reson. 138*, 334−342.
(41) Salinas, R. K., Bruschweiler-Li, L., Johnson, E., and Brüschweiler, R. (2011) Ca2+ binding alters the interdomain flexibility between the two cytoplasmic calcium-binding domains in the Na+/Ca2+ exchanger. *J. Biol. Chem. 286*, 32123−32131.
(42) Hus, J. C., Salmon, L., Bouvignies, G., Lotze, J., Blackledge, M., and Brüschweiler, R. (2008) 16-fold degeneracy of peptide plane orientations from residual dipolar couplings: analytical treatment and implications for protein structure determination. *J. Am. Chem. Soc. 130*, 15927−15937.
(43) Losonczi, J. A., Andrec, M., Fischer, M. W. F., and Prestegard, J. H. (1999) Order matrix analysis of residual dipolar couplings using singular value decomposition. *J. Magn. Reson. 138*, 334−342.
(44) Shen, Y., and Bax, A. (2013) Protein backbone and sidechain torsion angles predicted from NMR chemical shifts using artificial neural networks. *J. Biomol. NMR 56*, 227−241.
(45) Skrynnikov, N. R., Goto, N. K., Yang, D., Choy, W. Y., Tolman, J. R., Mueller, G. A., and Kay, L. E. (2000) Orienting domains in proteins using dipolar couplings measured by liquid-state NMR: differences in solution and crystal forms of maltodextrin binding protein loaded with beta-cyclodextrin. *J. Mol. Biol. 295*, 1265−1273.
(46) Delaglio, F., Kontaxis, G., and Bax, A. (2000) Protein Structure Determination Using Molecular Fragment Replacement and NMR Dipolar Couplings. *J. Am. Chem. Soc. 122*, 2142−2143.
(47) Fischer, M. W., Losonczi, J. A., Weaver, J. L., and Prestegard, J. H. (1999) Domain orientation and dynamics in multidomain proteins from residual dipolar couplings. *Biochemistry 38*, 9013−9022.
(48) Clore, G. M. (2000) Accurate and rapid docking of protein-protein complexes on the basis of intermolecular nuclear overhauser

DOI: 10.1021/acs.biochem.5b00420
Biochemistry 2015, 54, 5095−5102

enhancement data and dipolar couplings by rigid body minimization. *Proc. Natl. Acad. Sci. U. S. A. 97*, 9021−9025.
(49) Blackledge, M. (2005) Recent progress in the study of biomolecular structure and dynamics in solution from residual dipolar couplings. *Prog. Nucl. Magn. Reson. Spectrosc. 46*, 23−61.
(50) Chen, K., and Tjandra, N. (2011) The use of residual dipolar coupling in studying proteins by NMR. *Top Curr. Chem. 326*, 47−67.
(51) Bax, A. (2003) Weak alignment offers new NMR opportunities to study protein structure and dynamics. *Protein Sci. 12*, 1−16.
(52) McIntosh, D. B., Clausen, J. D., Woolley, D. G., MacLennan, D. H., Vilsen, B., and Andersen, J. P. (2004) Roles of conserved P domain residues and Mg2+ in ATP binding in the ground and Ca2+-activated states of sarcoplasmic reticulum Ca2+-ATPase. *J. Biol. Chem. 279*, 32515−32523.
(53) Voskoboinik, I., Mar, J., and Camakaris, J. (2003) Mutational analysis of the Menkes copper P-type ATPase (ATP7A). *Biochem. Biophys. Res. Commun. 301*, 488−494.
(54) Toyoshima, C. (2008) Structural aspects of ion pumping by Ca2+-ATPase of sarcoplasmic reticulum. *Arch. Biochem. Biophys. 476*, 3−11.

DOI: 10.1021/acs.biochem.5b00420
Biochemistry 2015, 54, 5095−5102